Available online at www.sciencedirect.com

ScienceDirect

Ceramics International 40 (2014) 2915–2926

CERAMICS INTERNATIONAL

www.elsevier.com/locate/ceramint

Influence of metal ion concentration in the glycol mediated synthesis of $Gd_2O_3:Eu^{3+}$ nanophosphor

R.G. Abhilash Kumar[a], Satoshi Hata[b], Ken-ichi Ikeda[b], K.G. Gopchandran[a,*]

[a]Department of Optoelectronics, University of Kerala, Thiruvananthapuram 695581, India
[b]Department of Electrical and Materials Science, Faculty of Engineering Sciences, Kyushu University, Kasuga, Fukuoka 816-8580, Japan

Received 2 September 2013; received in revised form 30 September 2013; accepted 4 October 2013
Available online 11 October 2013

Abstract

The solvothermal synthesis of highly luminescent and homogeneous $Gd_2O_3:Eu^{3+}$ nanophosphor using diethylene glycol as medium, followed by controlled combustion with citric acid as fuel is reported. The influence of concentrations of carboxylic acid and metal cations on the structure, morphology and luminescence properties are investigated in detail. The microscopic investigations indicate the nanocrystalline nature and the strong influence of cation concentration on the size, shape and agglomeration of the particles. It is found that increase in concentration of metal cations lead to the reduction in agglomeration of nanophosphors. The large value of intensity parameter Ω_2, suggested that Eu^{3+} ions reside in a more asymmetric environment, resulted in intense emission due to $^5D_0$–$^7F_2$ electric dipole transition. Emission decay analysis of the samples exhibited one exponential nature. The samples prepared under optimum conditions showed a quantum efficiency of 78.63% and a moderately high life time of 1.217 ms.
© 2013 Elsevier Ltd and Techna Group S.r.l. All rights reserved.

Keywords: A. Powders: chemical preparation; B. Grain size; C. Lifetime; C. Optical properties; Gd_2O_3

1. Introduction

Luminescent nanomaterials with high degree of homogeneity by reliable synthesis routes resulting in defined size, lesser defects and fewer impurities are essential for prospective optoelectronic device applications. Inorganic light emitting materials, namely phosphors have been widely studied by various researchers for applications in high definition television (HDTV), plasma display panels (PDP), cathode ray tube (CRT), flat panel displays (FPD), fluorescent lamps, lighting, medical diagnostics, sensing, defence security ink applications and field emission displays (FED) [1,2]. In the synthesis of phosphors for device applications, the prime areas concerned are morphology, stoichiometry, composition and surface chemistry and for practical applications, high brightness and quantum efficiency are expected [3,4]. In nanophosphors, lattice and surface defects form non-radiative relaxation channels like surface-adsorbed groups resulting in quenching during radiative transition. Interest in rare earth ion doped phosphors is mainly because of their ability to produce visible emission by down and up-conversion processes. Luminescence efficiency of these materials is often limited by the dynamics of the rare earth ions, which depend on the interaction between the rare earth ions and the host, such as local environment around the dopants, concentration of dopants, distribution of activator ions in the host material and the energy transfer from the host to the active ions.

Among rare earth oxides, gadolinium oxide (Gd_2O_3) is a promising host material for both down and up-conversion luminescence applications due to its high density, good chemical durability, thermal stability, photochemical stability and low phonon energy [5–16]. $Gd_2O_3:Eu^{3+}$ is paramagnetic with rich emission properties and is employed in fluorescence lamps, projection television tubes, biological fluorescent labelling, lighting, contrasting agent in magnetic resonance imaging and display applications [1,17–21]. Europium ions can substitute the Gd^{3+} sites in $Gd_2O_3:Eu^{3+}$ and occupy the lattice

*Corresponding author. Tel.: +91 4712308167.
E-mail address: gopchandran@yahoo.com (K.G. Gopchandran).

0272-8842/$ - see front matter © 2013 Elsevier Ltd and Techna Group S.r.l. All rights reserved.
http://dx.doi.org/10.1016/j.ceramint.2013.10.020

sites C_2 and S_6 in cubic phase. Eu^{3+} doped Gd_2O_3 exhibits bright red emission by activating the trivalent rare earth ion Eu^{3+}, through different sensitization processes such as the host Gd_2O_3 absorption, Gd^{3+} ion absorption, Eu–O charge transfer and the Eu^{3+} ion self excitation. For the efficient emission by down conversion, one of the popular ways to sensitize the rare earth emission is through excitation by charge transfer band (CTB). The absorbed energy in CTB is then transferred to the rare earth ions through non-radiative relaxation process.

Usually, luminescent properties like emission lifetime, quantum efficiency and concentration quenching depend on the size and morphology of the phosphor [22,23]. Chemical synthesis routes, like co-precipitation, sol–gel, hydrothermal, combustion methods or synthesis through aerosol offer many advantages over conventional approaches. The precursors are uniformly mixed at the molecular level in a solution based synthesis method giving a high degree of structural homogeneity in the phosphor. Rare earth ion incorporated Gd_2O_3 phosphors have been synthesized in various morphologies like spheres, plates, rods, nanotubes, nanowires, 3D flowers and thin films by a number of techniques such as sol–gel methods, aerosol routes, co-precipitation methods, molten salt routes, chemical vapour deposition, pulsed laser deposition, hydrogen flame pyrolysis methods, non-hydrolytic high temperature methods, combustion methods, spray pyrolysis and hydrothermal routines [5,8,24–33].

Recently, diethylene glycol assisted synthesis of europium incorporated Gd_2O_3 nanophosphor with high degree of homogeneity and enhanced emission was reported [34]. Citric acid has already been employed as shape modifiers to adjust and control the size and morphology of nanoparticles [35,36]. Herein, the dependence of metal cations concentration on the structure, morphology and luminescence of Eu^{3+} doped Gd_2O_3 nanophosphor prepared by solvothermal combustion in diethylene glycol medium is discussed. In this method, citric acid acts as a chelating agent to metal cations via the hydroxyl and carboxyl groups. Judd–Ofelt analysis has been used to obtain the radiative properties of the samples from the emission spectra and dynamic life time measurements.

2. Experimental

Materials used for synthesis were gadolinium oxide (Gd_2O_3, 99.99%, Aldrich), europium oxide (Eu_2O_3, 99.99%, Aldrich), conc. HNO_3 (70%, Merck), polyethylene glycol 200 (PEG, 99%, Merck), diethylene glycol (DEG, $C_4H_{10}O_3$, Merck, 99%) and citric acid monohydrate ($C_6H_8O_7 \cdot H_2O$, A.R. grade). Stoichiometric amounts of Eu_2O_3 and Gd_2O_3 corresponding to the composition $Gd_{1.9}Eu_{0.1}O_3$ were dissolved in concentrated nitric acid and deionized water ($1HNO_3$:$1H_2O$) to prepare their respective nitrate solutions. The solutions were then uniformly mixed by magnetic stirring and citric acid in diethylene glycol was added slowly into the prepared aqueous nitrate solution to chelate metal ions to form metal–citrate complex. The molar concentration ratio of citric acid to metal cations (CM ratio) was varied from 0.5:1 to 3:1 and 2 ml of polyethylene glycol was added to this solution as mineraliser. The mixed solution was then kept at a temperature of about 100 °C with continuous stirring in a water bath until a highly transparent viscous solution is obtained. The resulting viscous solution is then kept at 180 °C for 1 h followed by controlled combustion at 400 °C to obtain greyish precursor. Fully ground precursors were then subjected to sintering at 800 °C for 2 h to obtain the Eu^{3+} doped Gd_2O_3 nanophosphors.

Crystal structure and phase formation of the phosphors were examined using an X-ray diffractometer (Philips PANalytical X'pert Pro) operating at 40 kV and 30 mA with Cu Kα radiation (λ=1.54056 Å) employing X'Celerator and monochromator at the diffracted beam side in the angular range 2θ from 10 to 60°. Phase identification of the samples was performed using the X'Pert Highscore Software along with ICDD-PDF2 database. Low and high resolution transmission electron microscopy (TEM) and selected area electron diffraction (SAED) studies were performed using a FEI Tecnai F20 electron microscope with a field emission gun, operating at 200 KV. The infrared (IR) vibrational spectra of the samples were done in the wavenumber range 400–4000 cm^{-1} by a Fourier Transform Infrared (FTIR) Spectrometer (Shimadzu IRPrestige-21) using the KBr pellet method. The diffuse reflectance (DRS) measurements were carried out on a UV–visible spectrophotometer (JASCO V550) equipped with an integrating sphere (ISV-469) attachment and $BaSO_4$ was used as the reference for measurements to evaluate the band gaps. The Raman spectra of all samples were recorded in backscattering geometry using a confocal micro Raman spectrometer system (Horiba Jobin-Yvon LABRAM-HR800) equipped with a semiconductor diode laser having 785 nm emission (current of 198 mA) and employing a peltier cooled CCD detector. Jobin-Yvon Horiba Fluorolog (FL3-11) Spectrofluorophotometer equipped with a 450 W xenon lamp as the excitation source and a photomultiplier tube in photon counting mode (Hamamatsu R928P) as detector was used to record the excitation and emission spectra at room temperature. The lifetime measurements were recorded using decay by delay method with a FL-1040 phosphorimeter attachment to spectrofluorophotometer employed with microsecond pulsed xenon lamp as the source of excitation. The CIE colour coordinates (x, y) and correlated colour temperature (CCT) of the samples were estimated from the photoluminescent emission spectra based on the 1931 CIE 2 degree colour matching functions. Judd–Ofelt and radiative parameters of the synthesized phosphors were evaluated from the respective emission spectra and dynamic life time measurements.

3. Results and discussion

3.1. Phase analysis, crystal structure and morphology studies

Fig. 1 shows the X-ray diffraction patterns of $Gd_{1.9}Eu_{0.1}O_3$ samples synthesized at 800 °C with different citric acid to metal cation concentration ratios. All the peaks in the diffraction patterns are indexed according to JCPDS file of cubic Gd_2O_3 (JCPDS File no. 12-0797, Ia3 (206) space group, cell

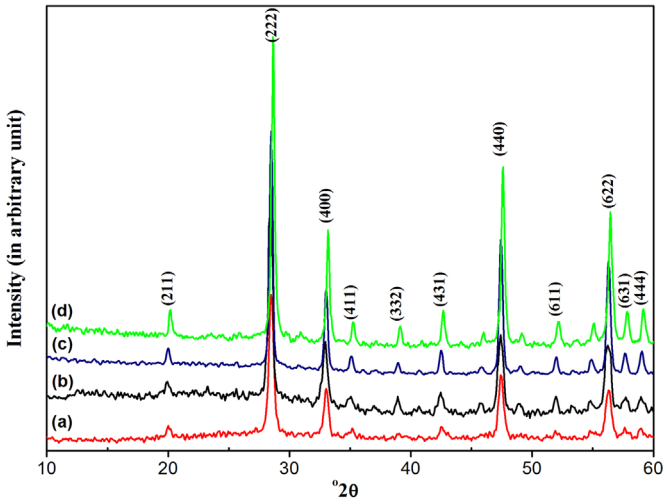

Fig. 1. XRD patterns of $Gd_{1.9}Eu_{0.1}O_3$ nanophosphors synthesized with different citric acid to metal cations molar concentration ratios (a) 0.5:1, (b) 1:1, (c) 2:1 and (d) 3:1.

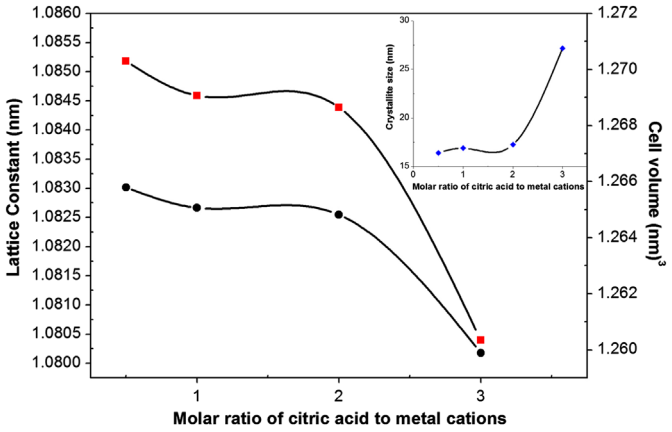

Fig. 2. Variation of lattice parameters [inset: crystallite size] of $Gd_{1.9}Eu_{0.1}O_3$ nanophosphors synthesized with different molar concentrations ratio of citric acid to metal cations.

parameter $a = 1.0813$ nm). The ionic radius of the Eu^{3+} and Gd^{3+} are 0.0947 and 0.0938 nm and the closeness of these values make the substitution process easier. The intensity of X-ray diffraction patterns are found to increase with increase in citrate concentration. The lattice constant (a) of the samples were calculated from the lattice spacing (d) of the hkl crystal planes using the equation of cubic system given by

$$\frac{1}{d^2} = \frac{(h^2+k^2+l^2)}{a^2} \quad (1)$$

The crystallite size of the samples were calculated from XRD patterns using the Debye–Scherrer equation

$$\text{Crystallite size } (D_{hkl}) = \frac{K\lambda}{\beta_{hkl}\cos\theta_{hkl}} \quad (2)$$

where K is a constant ($=0.9$), λ is the wavelength of X-rays used (0.154056 nm), β is the diffracted full width at half maximum (FWHM) in radian, θ is the Bragg diffraction angle and D_{hkl} represents the size along (hkl) direction. The dependence of lattice constant, cell volume and crystallite size of the samples prepared with different metal ion concentrations are shown in Fig. 2.

TEM and SAED images shown in Fig. 3(a)–(d) and (e)–(h) correspond to nanophosphors prepared with citric acid to metal cations concentration ratios 2:1 and 3:1 respectively. Both TEM images indicate that the nanoparticles posses high degree of homogeneity in size and shape with a length scale of 25 ± 2 nm and 31 ± 2 nm for samples respectively, and are in agreement with the values obtained from the X-ray diffraction analysis. It is well known that spherical shaped grains are potentially important because of their lower scattering of light, high packing density and better luminescence properties for device applications [1]. The HRTEM and SAED patterns show the nanocrystalline nature of the samples with interplanar spacing of 0.312 nm and 0.311 nm respectively, which corresponds to the spacing of the (222) lattice planes of cubic Gd_2O_3. The indexed SAED patterns are in good agreement with the observations made in the X-ray diffraction patterns and reveal the strong influence of citrate concentration in the crystallinity of the samples.

3.2. Optical studies

The Kubelka–Munk analysis [37] was used to calculate the band gap of the nanophosphors from the diffuse reflectance spectra of the samples. For this, the Kubelka–Munk function ($F(R_\infty)$) was used to convert the reflectance of the sample (R_{sample}), normalised by the reflectance of the reference ($R_{reference}$), into an equivalent absorption spectrum. The relation between the diffuse reflectance of the sample (R_∞), absorption coefficient (K) and scattering coefficient (S) is given by the K–M function $F(R_\infty)$ as

$$\frac{K}{S} = \frac{(1-R_\infty)^2}{2R_\infty} \equiv F(R_\infty) \quad (3)$$

$$F(R_\infty)h\nu \propto (h\nu - E_g)^n \quad (4)$$

where $R_\infty = R_{sample}/R_{reference}$, $h\nu$ is the incident photon energy and the value of n, depends on the type of optical transition caused by the photon absorption. Fig. 4 shows the variation of square of the Kubelka–Munk function multiplied by the photon energy with photon energy for the samples. The calculated value of band gap energy of the prepared nanophosphors was obtained to be in the range 5.66–5.68 eV.

Fig. 5 shows the FTIR transmission spectra of $Gd_{1.9}Eu_{0.1}O_3$ nanophosphors synthesized with different molar ratio of citric acid to metal cations. The absorption band around 3420 cm^{-1} corresponds to the stretching vibration of O–H which provides evidence of water of hydration in the structure or it may be due to surface adsorbed water from atmosphere and the dispersant KBr during the course of infra-red measurement [38]. The peaks around 1400 and 1510 cm^{-1} are due to C–O bond vibrations and these peaks are due to residual carbon in the prepared samples or absorption of CO_2 from the ambient atmosphere [38,39]. The absorption bands at 544 and 440 cm^{-1} can be assigned to be the typical Gd–O vibration

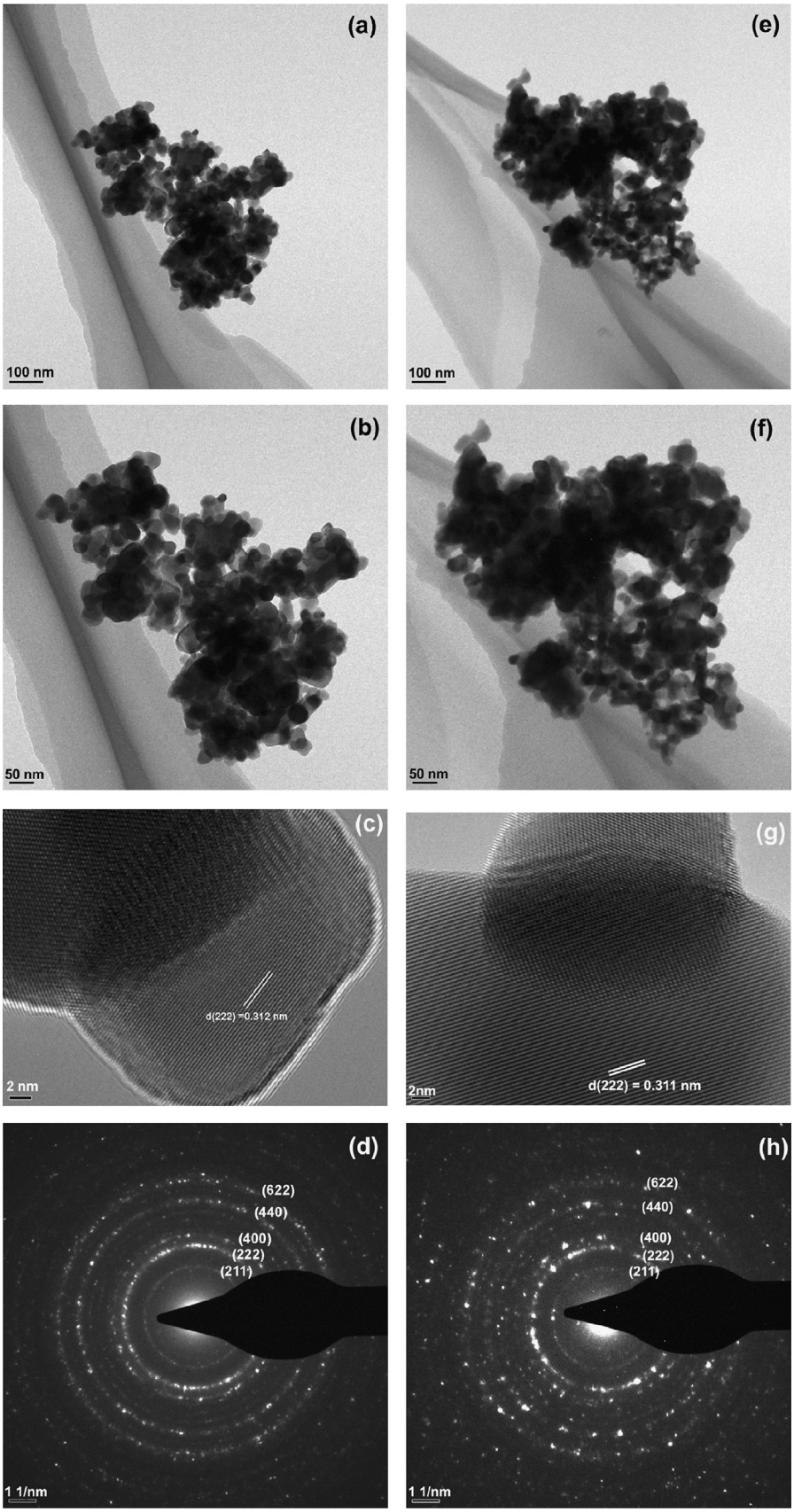

Fig. 3. TEM images and SAED patterns of $Gd_{1.9}Eu_{0.1}O_3$ nanophosphors prepared with different molar concentration ratios of citric acid to metal cations (a)–(d) 2:1 and (e)–(h) 3:1.

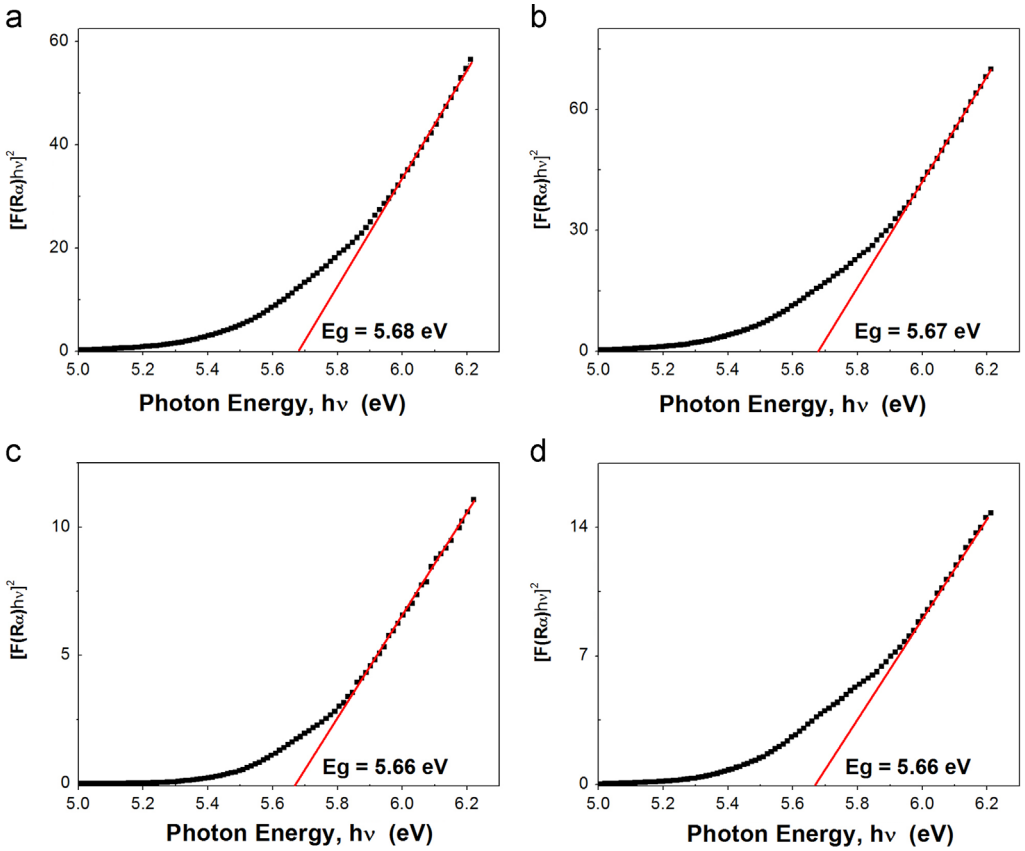

Fig. 4. Kubelka–Munk $[(F(R\alpha)h\nu)^2$ vs photon energy] plots of the $Gd_{1.9}Eu_{0.1}O_3$ nanophosphors synthesised with different citric acid to metal cations molar concentration ratios (a) 0.5:1, (b) 1:1, (c) 2:1 and (d) 3:1.

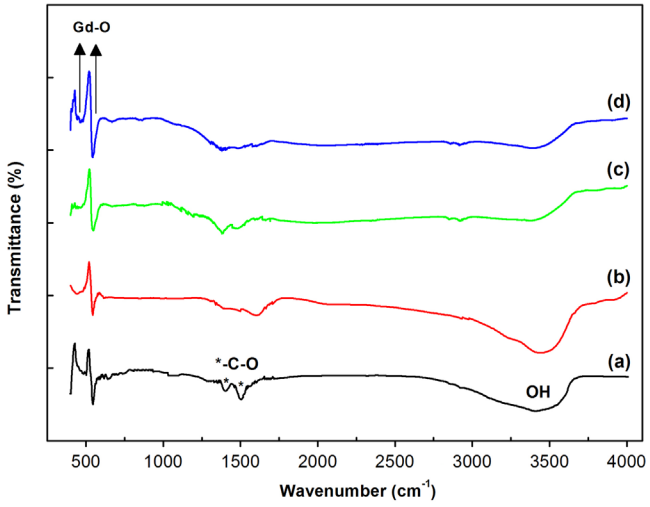

Fig. 5. FTIR spectra of $Gd_{1.9}Eu_{0.1}O_3$ nanophosphors synthesized with different citric acid to metal cations molar concentration ratios (a) 0.5:1, (b) 1:1, (c) 2:1 and (d) 3:1.

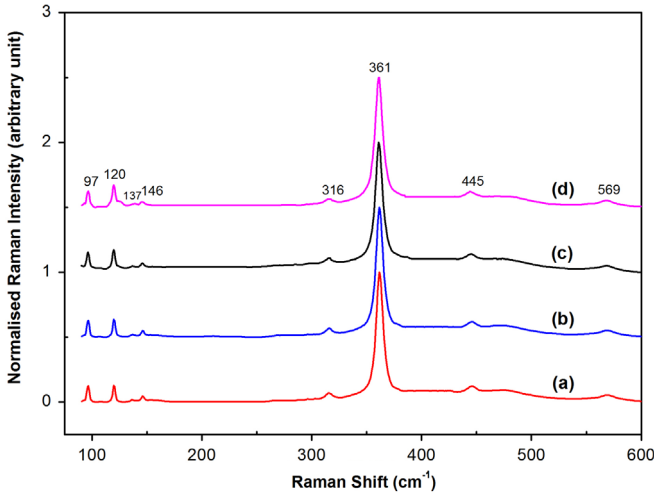

Fig. 6. Normalised Raman spectra of $Gd_{1.9}Eu_{0.1}O_3$ nanophosphors synthesized with different citric acid to metal cations molar concentration ratios (a) 0.5:1, (b) 1:1, (c) 2:1 and (d) 3:1.

of cubic Gd_2O_3 [40] and the intensity of these vibrational bands is found to increase with increase in molar concentration of citric acid, indicating increase of crystallinity and grain growth, as evidenced in XRD and TEM measurements.

The Raman scattering is very sensitive to the lattice vibrations and any structural modifications present in the samples. The normalised micro Raman spectrum of $Gd_{1.9}Eu_{0.1}O_3$ samples synthesized with different citric acid to metal cations molar concentrations are shown in Fig. 6. Gd_2O_3 is a C-type rare earth sesquioxide (isostructural to Y_2O_3) body centred cubic with space group Ia3, Th^7, $Z=16$. The structure has 32 cations, of which 8 RE^{3+} ions are on the b sites with

symmetry S_6 and 24 RE^{3+} ions on the d sites with point symmetry C_2 and the 48 oxygen anions are on the e sites with point symmetry C_1 [41]. The irreducible representations for the optical and acoustical modes by factor group analysis [41,42] can be generally expressed as

$$\Gamma_{op} = 4A_g + 4E_g + 14F_g + 5A_{2u} + 5E_u + 16F_u, \Gamma_{ac} = F_u \qquad (5)$$

where A_g, E_g, and F_g are Raman active, F_u is Infrared active and A_{2u} and E_u are inactive. All the samples showed Raman vibrations located at 97, 120, 135, 145, 316, 361, 445 and 569 cm^{-1} corresponding to cubic Gd_2O_3, consistent with the values reported by Luyer et al. [43] and no significant change in the position of Raman peaks is observed. The intense Raman band at 361 cm^{-1} corresponds to Fg + Ag mode of vibration having large polarizability change [43].

3.3. Luminescence, Judd–Ofelt and radiative analysis

Fig. 7 shows the photoluminescent excitation spectra of the $Gd_{1.9}Eu_{0.1}O_3$ nanophosphors monitoring the emission at 612 nm (λ_{em} = 612 nm) corresponding to $^5D_0$–$^7F_2$ transition. All the excitation spectra consist of a strong broad band in the wavelength range 220–300 nm with a maximum at 265 nm caused by the charge transfer (CT) electronic transition from the 2p orbital of O^{2-} to the empty 4f orbital of the central Eu^{3+} ions [1], position of which depends on the covalency between O^{2-} and Eu^{3+}, Eu–O bond length, bond volume polarisation, charge of the ligand in the chemical bond and coordination number of central Eu^{3+} ion [44–46]. Weak excitation lines observed at 276, 278 and 280 nm is due to the $^8S_{7/2}$–$^6I_{7/2-17/2}$ and 314 nm is due to $^8S_{7/2}$–$^6P_{3/2-7/2}$ intra f–f transitions of Gd^{3+} ion. The presence of these lines in the excitation spectrum shows the occurrence of energy transfer from Gd^{3+} to Eu^{3+} activator ions in the samples [47]. Sharp excitation lines beyond 320 nm belong to the intrinsic f–f transitions of Eu^{3+} within its $4f^6$ configurations, which is shielded from environmental effects by the outer shell electrons [1] and are assigned as the electronic transitions of $^7F_0$–$^5H_6$ at 323 nm, $^7F_0$–$^5D_4$ at 364 nm, $^7F_0$–$^5G_{2-6}$ at 383 nm, $^7F_0$–$^5L_6$ at 395 nm, $^7F_0$–$^5D_3$ at 416 nm, $^7F_0$–$^5D_2$ at 467 nm and $^7F_0$–$^5D_1$ at 533 nm [12]. Comparing the excitation spectra of the samples, the intensity is found to be maximum for the sample prepared with CM ratio of 2:1.

Rare earth ions in host matrix usually give sharp emission lines due to the transitions within the 4f shell and are forbidden, but allowed due to the surrounding crystal field relaxation in the selection rules. Emission spectra of samples prepared with different molar concentrations of citric acid to metal cations are shown in Fig. 8. All these spectra consists of five groups of distinctive emission peaks between 550 and 720 nm, corresponding to the electronic transitions from the excited $^5D_0$ to ^7F_J (J=0, 1, 2, 3, 4) levels of Eu^{3+} ions [48] and are assigned to the $^5D_0$–$^7F_0$ (581 nm), $^5D_0$–$^7F_1$ (588, 593 and 599 nm), $^5D_0$–$^7F_2$ (612 and 630 nm), $^5D_0$–$^7F_3$ (651 nm) and $^5D_0$–$^7F_4$ (707 nm). Fig. 9 shows the partial energy level diagram of Gd_2O_3:Eu^{3+} nanophosphor describing the excitation and emission mechanisms. The intensity of transitions

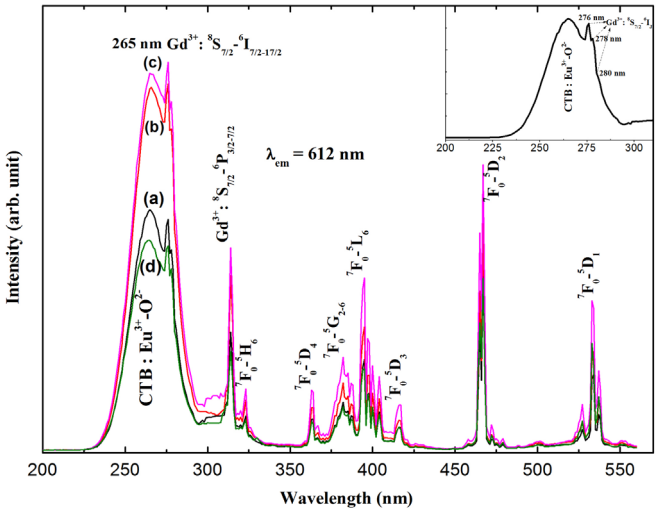

Fig. 7. Excitation spectra of $Gd_{1.9}Eu_{0.1}O_3$ nanophosphors synthesized with different citric acid to metal cations molar concentration ratios (a) 0.5:1, (b) 1:1, (c) 2:1 and (d) 3:1 (inset shows the expanded view of Fig. 7(c)).

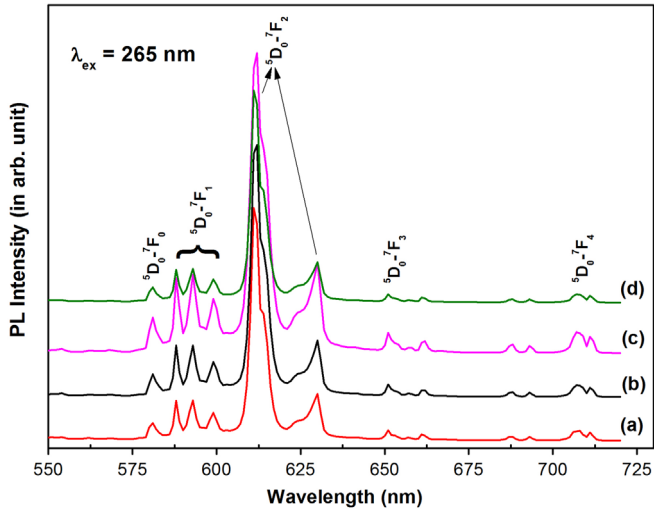

Fig. 8. Emission spectra of $Gd_{1.9}Eu_{0.1}O_3$ nanophosphors synthesized with different citric acid to metal cations molar concentration ratios (a) 0.5:1, (b) 1:1, (c) 2:1 and (d) 3:1; under CTB excitation of 265 nm.

between different J levels depends on the symmetry of the local environment of Eu^{3+} activators and can be determined from Judd–Ofelt theory [49]. For Eu^{3+} ions incorporated phosphors, the structure of the host and the lattice site of Eu^{3+} ions are crucial factors that can affect the emission characteristics. In cubic Gd_2O_3 lattice, Eu^{3+} ions can occupy two sites: one is the 24d site with C_2 point non-inversion symmetry and another is the 8b site with S_6 point inversion symmetry and the ratio between them is 3:1 and its occupancy in both these sites are evident in the emission spectrum (Fig. 8). If Eu^{3+} is located in a site S_6 with an inversion centre, the $^5D_0$–$^7F_1$ with ΔJ=1, magnetic dipole transition should be dominant, otherwise in a site C_2 without an inversion centre, the $^5D_0$–$^7F_2$ electric dipole transition will be predominant. The observed peak at 612 nm corresponds to the hypersensitive forced

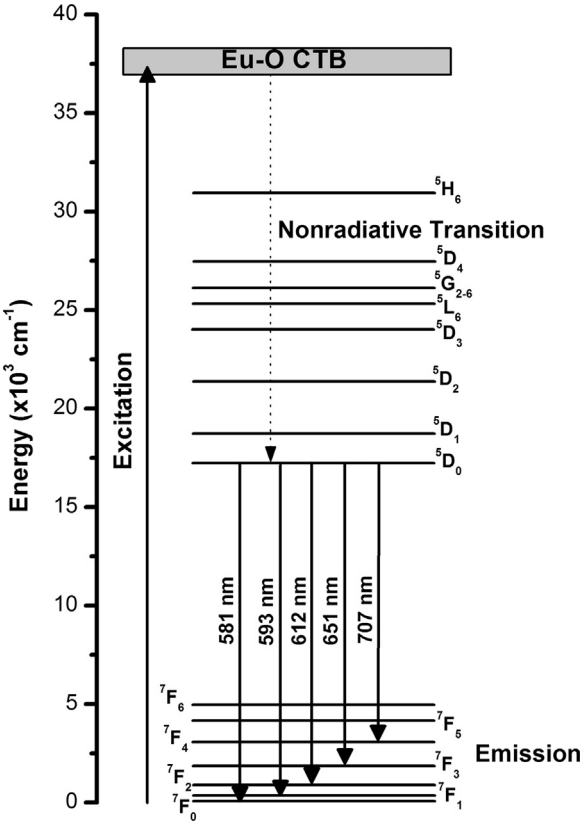

Fig. 9. Partial energy level diagram of Gd_2O_3:Eu^{3+} nanophosphor showing the excitation and emission mechanisms.

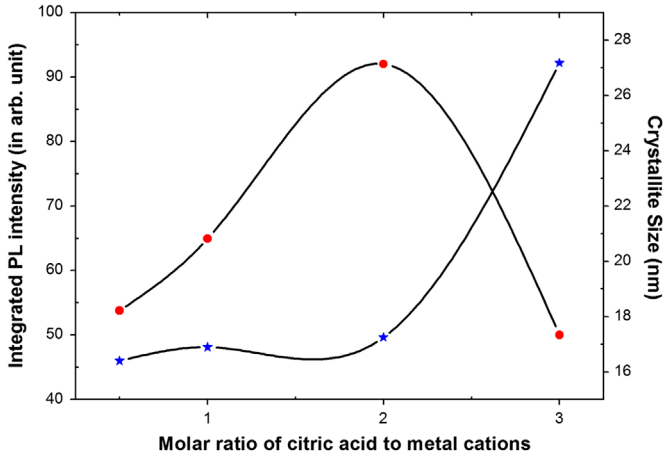

Fig. 10. Variation of grain size and the integrated emission intensity of $Gd_{1.9}Eu_{0.1}O_3$ nanophosphors as a function of molar concentration ratio of citric acid to metal cations.

electric dipole $^5D_0$–$^7F_2$ transition of Eu^{3+} ion with the selection rule $\Delta J=2$ [1], which in turn results in higher colour purity of red emission. The dependence of intensity of emission of samples on the concentration of metal cations is shown in Fig. 10. It is found that the intensity of emission increases with increase in citric acid concentration and reaches a maximum for the sample synthesized with citric acid to metal

Table 1
Values of CIE chromaticity coordinates (x, y) and correlated colour temperature (CCT) evaluated from the emission spectra of $Gd_{1.9}Eu_{0.1}O_3$ samples.

Sample	Molar ratio of citric acid to metal cations	CIE coordinates		CCT (K)
		x	y	
a	0.5:1	0.6292	0.3537	1997
b	1:1	0.6327	0.3537	2027
c	2:1	0.6341	0.3530	2052
d	3:1	0.6317	0.3524	2039

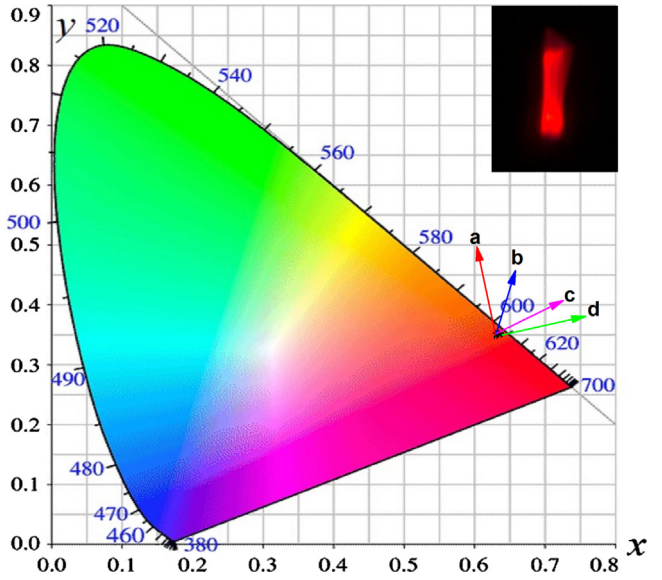

Fig. 11. CIE chromaticity diagram showing the coordinates for the emission spectra of $Gd_{1.9}Eu_{0.1}O_3$ nanophosphor synthesized with different molar concentration ratios of citric acid to metal cations (inset: photograph of the sample under 256 nm, 4 W UV lamp illumination).

cations molar ratio of 2:1. For samples synthesized with lower citric acid concentration, grain size of the samples obtained is small giving rise to larger surface area and the large surface area introduces a number of defects into the nanophosphor, resulting in lesser intensity of emission [12].

Earlier studies on the local structure of nanophosphors reveal that the local structure changes and becomes more complicated when the size of particles decreases to nanoscale [50]. Particularly for Eu^{3+} doped phosphors, the ratio of the integrated intensities of the $^5D_0$–$^7F_2$ hypersensitive electric dipole transition to the $^5D_0$–$^7F_1$ magnetic dipole transition is considered as an indicator of the asymmetry and the crystal field environment around the Eu^{3+} ions, expressed as asymmetry ratio (A or R_{21}) [1]. This ratio is influenced by cation site occupancies, distortion of the lattice, and the nanocrystalline nature of the sample [51]. If $R_{21} > 1$, it indicate an asymmetric environment around the Eu^{3+} ion and consequently a larger local disorder of the lattice [52]. The asymmetry ratios of the samples obtained are listed in Table 2, and it indicates that there is no significant change in symmetry with the concentration of metal cations.

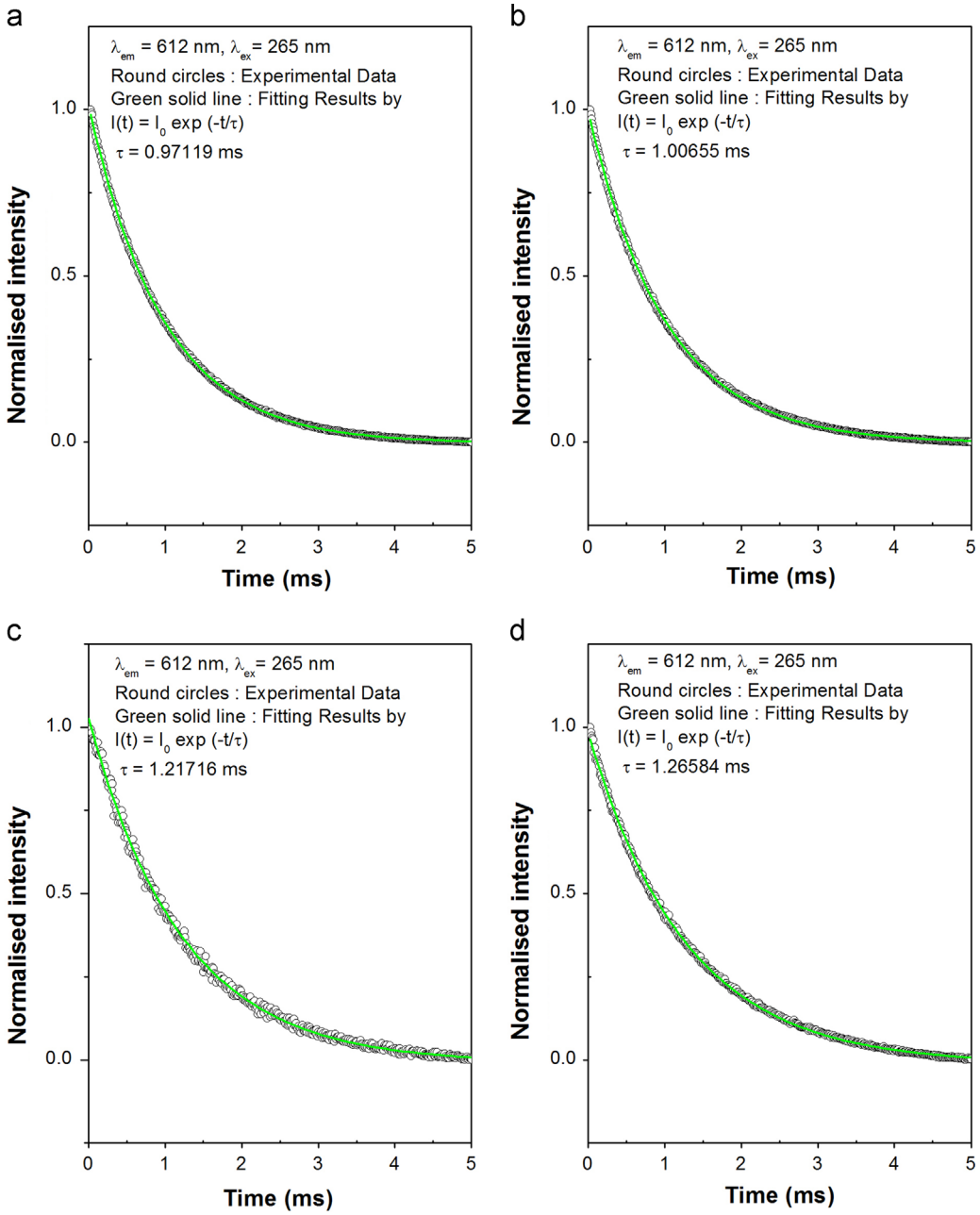

Fig. 12. Decay curves of $^5D_0$–$^7F_2$ transition at 612 nm of Eu^{3+} ions in $Gd_{1.9}Eu_{0.1}O_3$ nanophosphors synthesized with different citric acid to metal cations molar concentration ratios (a) 0.5:1, (b) 1:1, (c) 2:1 and (d) 3:1.

For device applications, in addition to the quantum efficiency and brightness, the colour chromaticity of the samples is a key parameter for performance evaluation of red phosphors and is studied using the Commission Internationale de L'Eclairage (CIE) in 1931 system [53]. Table 1 lists the CIE colour chromaticity coordinates (x, y) derived from the emission spectra of all the samples and the corresponding 1931 CIE chromaticity diagram is shown in Fig. 11. Chromaticity coordinates are useful in determining the exact emission colour and colour purity of the sample. The obtained CIE colour coordinates for the samples are in the standard red colour region. Correlated Colour Temperature (CCT), measured in Kelvin (K) has been used as a metric to characterise broad band light sources and in this investigation the CCT values are calculated employing the McCamy method [54] and are summarised in Table 1.

Fluorescence lifetime of the excited state provides information about different relaxation processes and the luminescent decay dynamic behaviour of phosphors is affected by a number of factors such as number of luminescent centres, energy transfer, defects and impurities present in the host. Luminescence decay dynamics for the $^5D_0$–$^7F_2$ transition of Eu^{3+} ion at 612 nm of all the samples are shown in Fig. 12. It is found that the experimental decay behaviour for all the

samples can be fitted well by a single exponential function as

$$I(t) = I_0 \exp\left(-\frac{t}{\tau}\right) \quad (6)$$

where I_0 is the initial emission intensity at $t=0$ and τ is the lifetime of the emission centre. The lifetime values obtained for the $^5D_0$ lowest excited state are given in Fig. 12 and is in consistent with the reported values for other Eu^{3+} doped Gd_2O_3 systems [5,8]. It is found that the value of life time becomes longer with increase in CM ratio and reaches a maximum life time value of 1.26584 ms for the sample prepared with a CM ratio of 3:1.

The Judd–Ofelt theory [55,56] was developed individually by Judd and Ofelt in 1962 and is used to characterise the optical transitions of trivalent rare earth ions in specific host environments. Usually, Judd–Ofelt (J–O) intensity parameters, Ω_λ (λ=2, 4, and 6) are calculated to ascertain the structural changes. These parameters are essential indicators in determining radiative potential of rare earth ions in different host materials, which are usually determined from the absorption spectrum. However, in the case of Eu^{3+} ion, the pure magnetic dipole transition $^5D_0$–$^7F_1$ allows to determine the intensity parameters from the emission spectrum. The values of Ω_2 and Ω_4 parameters are associated with short and long range effects, respectively. The value of Ω_2 is expected to increase with site asymmetry, increase in coordination number and decrease in bond length. The Ω_4 and Ω_6 parameters are more sensitive towards macroscopic properties, such as rigidity of the matrix, dielectric constant and viscosity in which lanthanide ion is situated. Here in, the J–O parameters and radiative properties were determined from the emission spectrum using the $^5D_0$–$^7F_1$ magnetic dipole transition of Eu^{3+} ion as the reference. According to J–O theory, the magnetic dipole transition rate (A_{01}) of $^5D_0$–$^7F_1$ transition of Eu^{3+} ion is given by

$$A_{01} = \frac{64\pi^4 \nu_1^3 n^3 S_{md}}{3h(2J+1)} \quad (7)$$

The electric dipole transition rates (A_{0J}) of $^5D_0$–^7F_J transition (J=2, 4 and 6) can be expressed as

$$A_{0J} = \frac{64\pi^4 \nu_J^3}{3h(2J+1)} e^2 \frac{n(n^2+2)^2}{9} \sum_{\lambda=2,4,6} \Omega_\lambda |\langle {}^5D_0 \| U^{(\lambda)} \| {}^7F_J \rangle|^2 \quad (8)$$

where A_{0J} is the coefficient of spontaneous emission, e is the charge of electron, ν_J is wavenumber of the respective transition, $(2J+1)$ equals 1 for $^5D_0$ transitions, h is the Planck's constant, S_{md} is the strength of the magnetic dipole $^5D_0$–$^7F_1$ transition, which is a constant and independent of the medium, being equal to 9.6×10^{-42} units [57], n is the effective refractive index of the prepared nanophosphor. The squared reduced matrix element $|\langle {}^5D_0 \| U^{(\lambda)} \| {}^7F_J \rangle|^2$ is independent of the chemical environment of the Eu^{3+} ion and are 0.00324, 0.00229 and 0.00023 for J=2, 4 and 6, respectively [10]. Since the transition rate of each energy level is directly proportion to the integral intensity of emission spectrum, and hence the ratio of electric dipole to magnetic dipole transition rate can be written as

$$\frac{\int I_J dv}{\int I_1 dv} = \frac{A_{0J}}{A_{01}} = \frac{e^2}{S_{md}} \frac{\nu_J^3}{\nu_1^3} \frac{(n^2+2)^2}{9n^2} \Omega_\lambda |\langle {}^5D_0 \| U^{(\lambda)} \| {}^7F_J \rangle|^2 \quad (9)$$

and hence Ω_2, Ω_4 and Ω_6 are computed. The emission of $^5D_0$–$^7F_6$ transition is located in the infrared region and is quite weak, which could not be experimentally detected here, hence Ω_6 couldn't be estimated.

The observed fluorescence lifetime τ_{obs} of $^5D_0$, radiative transition rate A_R and non-radiative transition rate A_{NR} are related as

$$\frac{1}{\tau_{obs}} = A_T = A_R + A_{NR} \quad (10)$$

where A_T is the total transition rate.

The total radiative transition probability (A_R) is obtained by summing over the radiative rates A_{0J} for each $^5D_0$–^7F_J transition and is given by

$$A_R = \sum_J A_{0J} = A_{01} \frac{\nu_{01}}{I_{01}} \sum_{J=0}^{4} \frac{I_{0J}}{\nu_{0J}} \quad (11)$$

where ν_{01} and ν_{0J} are the energy barycentre of the $^5D_0$–$^7F_1$ and $^5D_0$–^7F_J transitions, A_{01} is the Einstein's coefficient between $^5D_0$–$^7F_1$ levels, I_{0J} is the integrated area related to the corresponding $^5D_0$–^7F_J transition obtained from the emission spectra data.

As the coefficients for spontaneous emission is equal to the reciprocal of the radiative relaxation time (τ_{rad}),

$$\tau_{rad} = \frac{1}{\sum_J A_{0J}} = \frac{1}{A_R} \quad (12)$$

Quantum efficiency of the luminescent material can be expressed as the ratio of the number of photons emitted by the Eu^{3+} to that of number of photons absorbed by the Eu^{3+} and it is related with radiative and non-radiative processes. Using the measured lifetime τ_{obs}, along with the calculated radiative lifetime τ_{rad}, the luminescence quantum efficiency (η) of the $^5D_0$ level can be written as,

$$\eta = \frac{\tau_{obs}}{\tau_{rad}} = \frac{A_R}{A_R + A_{NR}} = \tau_{obs} A_R \quad (13)$$

The fluorescence branching ratio measures the percentage of emission for a given transition from a state with respect to all other transitions from that state and hence the relative amplitudes of the fluorescence transitions or fluorescence branching ratio (β_{0J}) corresponding to the emission from an excited level to its lower level is

$$\beta_{0J} = \frac{A_{0J}}{\sum A_{0J}} \quad (14)$$

Judd–Ofelt theory can successfully account for the stimulated emission cross-section, which is determined by the Fuchtbabauer–Landenburg method as

$$\sigma_{0J} = \frac{\lambda_p^4}{8\pi c n^2 \Delta\lambda_{eff}} A_{0J} \quad (15)$$

Table 2
Judd–Ofelt intensity parameters (Ω_2, Ω_4) and ratio of integrated emission intensities of the $^5D_0$–$^7F_0$ and $^5D_0$–$^7F_2$ (R_{02}), $^5D_0$–$^7F_2$ and $^5D_0$–$^7F_1$ (R_{21}), $^5D_0$–$^7F_4$ and $^5D_0$–$^7F_1$ (R_{41}) transitions from $^5D_0$ to the ^7F_J levels determined from emission spectra of $Gd_{1.9}Eu_{0.1}O_3$ samples.

Molar ratio of citric acid to metal cations	Refractive index	No J mixing		J mixing		R_{02}	R_{21}	R_{41}
		Ω_2 ($\times 10^{-20}$ cm^2)	Ω_4 ($\times 10^{-20}$ cm^2)	Ω_2 ($\times 10^{-20}$ cm^2)	Ω_4 ($\times 10^{-20}$ cm^2)			
0.5:1	1.9175	8.1084	1.0522	9.3826	1.1754	0.0276	5.5859	0.3323
1:1	1.8985	8.1974	1.0746	9.4856	1.2004	0.0292	5.6146	0.3374
2:1	1.7988	8.5140	1.2775	9.8520	1.4271	0.0323	5.6694	0.3900
3:1	1.7785	8.1428	0.9648	9.4224	1.0778	0.0247	5.3939	0.2930

Table 3
Transition rates (A_R, A_{NR} and A_T), life time (τ_{rad} and τ_{obs}), emission quantum efficiency (η), branching ratios (β_{01}, β_{02} and β_{04}) and stimulated emission cross-sections (σ_{01}, σ_{02} and σ_{04}) of the $Gd_{1.9}Eu_{0.1}O_3$ nanophosphors determined from their respective emission spectra and life time data.

Radiative parameter	Molar ratio of citric acid to metal cations			
	0.5:1	1:1	2:1	3:1
A_R (s^{-1})	762.42	744.71	646.01	585.44
A_{NR} (s^{-1})	267.25	248.78	175.57	204.55
A_T (s^{-1})	1029.66	993.49	821.58	789.99
τ_{rad} (ms)	1.31162	1.34280	1.54796	1.70812
τ_{obs} (ms)	0.97119	1.00655	1.21716	1.26584
η (%)	74.05	74.96	78.63	74.11
β_{01} (%)	13.351	13.267	13.008	13.874
β_{02} (%)	76.970	76.873	76.113	77.232
β_{04} (%)	5.290	5.337	6.048	4.847
σ_{01} (cm^2)	6.9683×10^{-22}	7.4294×10^{-22}	7.4297×10^{-22}	5.6612×10^{-22}
σ_{02} (cm^2)	3.8465×10^{-21}	3.8833×10^{-21}	3.9801×10^{-21}	3.7440×10^{-21}
σ_{04} (cm^2)	4.5998×10^{-22}	4.9169×10^{-22}	5.9459×10^{-22}	3.9867×10^{-22}

where λ_p is the wavelength of peak emission and $\Delta\lambda_{eff}$ the effective line width of the emission band.

Table 2 presents the Judd–Ofelt intensity parameters of the samples together with the emission intensity ratios of the major electronic transitions from the $^5D_0$ level of Eu^{3+} to ^7F_J levels. The values of Judd–Ofelt intensity (J–O) parameters reflect the local structure and bonding in the vicinity of rare earth ions. According to Judd–Ofelt theory, electronic transitions from the $^5D_0$ state to low-lying ^7F_J levels with $J=0$, 3 or 5 are both electrically and magnetically forbidden in the frame of intermediate coupling scheme [55,56]. However the observed weak transitions from $^5D_0$ to these levels in the emission spectrum may be due to the crystal field induced J-mixing effect [10]. The R_{02} intensity parameter (Table 2), defined as the ratio between the intensities of the $^5D_0$–$^7F_0$ and $^5D_0$–$^7F_2$ transitions, may give information about the J-mixing effect associated with the $^5D_0$–$^7F_0$ transition. This effect is primarily due to the mixing between the $^7F_2$ manifold and the $^7F_0$ level, through the rank two components of the ligand field. The calculated values of J–O parameters are at par with the reported values [10]. For comparison, J–O parameters are also determined by considering the J mixing effect and found that it slightly affects the determined J–O parameters. The value of Ω_2 is much larger than that of Ω_4 for all samples and the larger value of the Ω_2 parameter indicates that Eu^{3+} ions are located in a higher polarizable chemical environment. Moreover, Ω_2 can describe the dependence between rare earth ions and ligand anions on the covalency and give information about the asymmetry of the local environment of Eu^{3+} site [58]. Transition rates (A_R, A_{NR} and A_T), life time (τ_{rad} and τ_{obs}), quantum efficiency (η), branching ratios (β_{01}, β_{02} and β_{04}) and stimulated emission cross-sections (σ_{01}, σ_{02} and σ_{04}) of the samples determined from the emission spectra and life time measurements are given in Table 3. The phosphor synthesized with 2:1 molar concentration ratio of citric acid to metal cations has the highest quantum efficiency of 78.63%. The obtained large value of emission cross-section for forced $^5D_0$–$^7F_2$ electric dipole transition indicates colour purity and lower symmetry of Eu^{3+} ions.

4. Conclusions

In summary, Eu^{3+} ion incorporated Gd_2O_3 nanophosphors were synthesized by solvothermal combustion of metal–citrate complex in diethylene glycol medium. The dependence of molar concentration ratio of citric acid to metal cations on the crystal structure, morphology and luminescence properties was investigated. X-ray diffraction and microscopic analysis

indicated strong influence of CM ratio on the crystallinity and morphology of the phosphor. Calorimetric parameters such as correlated colour temperature and CIE colour coordinates were evaluated and it was found that emission from nanophosphors lies in the red region. An optimum molar concentration ratio of 2:1 between citric acid to metal cations resulted in the formation of sample with a quantum efficiency of 78.63% and a life time of 1.217 ms. The life time decay dynamics of samples followed a single exponential function and life time value was found to be sensitive to molar concentration of metal cations. The larger value of the intensity parameter Ω_2, obtained from Judd–Ofelt analysis suggest that Eu^{3+} ions reside at a more asymmetric environment with higher covalency in the host matrix resulting in intense $^5D_0$–$^7F_2$ electric dipole transition. The present study suggests that molar concentration of metal cations plays a vital role in the morphology and structural environment of Eu^{3+} ion which modifies the radiative and non-radiative relaxations and the emission properties.

Acknowledgement

R.G. Abhilash Kumar acknowledges University Grants Commission (UGC), India for the award of teacher fellowship under the faculty development programme.

References

[1] G. Blasse, B.C. Grabmaier, Luminescent Materials, Springer-Verlag, Berlin, 1994.
[2] C. Feldmann, T. Justel, C.R. Ronda, P.J. Schmidt, Inorganic luminescent materials: 100 years of research and application, Adv. Funct. Mater. 13 (2003) 511–516.
[3] A. Vecht, C. Gibbons, D. Davies, X.P. Jing, P. Marsh, T. Ireland, J. Silver, A. Newport, D. Barber, Engineering phosphors for field emission displays, J. Vac. Sci. Technol. B 17 (1999) 750–757.
[4] G. Wakefield, E. Holland, P.J. Dobson, J.L. Hutchison, Luminescence properties of nanocrystalline Y_2O_3:Eu, Adv. Mater. 13 (2001) 1557–1560.
[5] L.Q. Liu, E. Ma, R.F. Li, G.K. Liu, X.Y. Chen, Effects of phonon confinement on the luminescence dynamics of Eu^{3+} in Gd_2O_3 nanotubes, Nanotechnology 18 (2007) 015403.
[6] A.G. Macedo, R.A.S. Ferreira, D. Ananias, M.S. Reis, V.S. Amaral, L.D. Carlos, J. Rocha, Effects of phonon confinement on anomalous thermalization, energy transfer, and upconversion in Ln^{3+}-doped Gd_2O_3 nanotubes, Adv. Funct. Mater. 20 (2010) 624–634.
[7] G. Jia, K. Liu, Y.H. Zheng, Y.H. Song, M. Yang, H.P. You, Highly uniform $Gd(OH)_3$ and Gd_2O_3:Eu^{3+} nanotubes: facile synthesis and luminescence properties, J. Phys. Chem. C 113 (2009) 6050–6055.
[8] G. Liu, G. Hong, J. Wang, X. Dong, Hydrothermal synthesis of spherical and hollow Gd_2O_3:Eu^{3+} phosphors, J. Alloys. Compd. 432 (2007) 200–204.
[9] L. Xu, Y. Yu, X. Li, G. Somesfalean, Y. Zhang, H. Gao, Z. Zhang, Synthesis and upconversion properties of monoclinic Gd_2O_3:Er^{3+} nanocrystals, Opt. Mater. 30 (2008) 1284–1288.
[10] L. Liu, X. Chen, Energy levels, fluorescence lifetime and Judd–Ofelt parameters of Eu^{3+} in Gd_2O_3 nanocrystals, Nanotechnology 18 (2007) 255704.
[11] K.M. Lin, Y.Y. Li, Luminescent properties and characterization of one dimensional Gd_2O_3:Eu^{3+} phosphor nano-wire for field emission application, Nanotechnology 17 (2006) 4048–4052.
[12] J. Yang, C.X. Li, Z.Y. Cheng, X.M. Zhang, Z.W. Quan, C.M. Zhang, J. Lin, Size-tailored synthesis and luminescent properties of one-dimensional Gd_2O_3:Eu^{3+} nanorods and microrods, J. Phys. Chem. C 111 (2007) 18148–18154.
[13] X. Chen, E. Ma, G. Liu, Energy levels and optical spectroscopy of Er^{3+} in Gd_2O_3 nanocrystals, J. Phys. Chem. C 111 (2007) 10404–10411.
[14] H. Guo, N. Dong, M. Yin, W.P. Zhang, L.R. Lou, S.D. Xia, Visible upconversion in rare earth ion-doped Gd_2O_3 nanocrystals, J. Phys. Chem. B 108 (2004) 19205–19209.
[15] S.V. Lechevallier, P. Lecante, R. Mauricot, H. Dexpert, J. Dexpert-Ghys, H.K. Kong, G.L. Law, K.L. Wong, Gadolinium–Europium carbonate particles: controlled precipitation for luminescent biolabeling, Chem. Mater. 22 (2010) 6153–6161.
[16] G. Glaspell, J. Anderson, J.R. Wilkins, M.S. El-Shall, Vapor phase synthesis of upconverting Y_2O_3 nanocrystals doped with Yb^{3+}, Er^{3+}, Ho^{3+}, and Tm^{3+} to generate red, green, blue, and white light, J. Phys. Chem. C 112 (2008) 11527–11531.
[17] M. Nichkova, D. Dosev, S.J. Gee, B.D. Hammock, I.M. Kennedy, Microarray immunoassay for phenoxybenzoic acid using polymer encapsulated Eu:Gd_2O_3 nanoparticles as fluorescent labels, Anal. Chem. 77 (2005) 6864–6873.
[18] E.M. Goldys, D.T. Krystyna, S. Jinjun, D. Dosev, I.M. Kennedy, S. Yatsunenko, M. Godlewski, Optical characterization of Eu-doped and undoped Gd_2O_3 nanoparticles synthesized by the hydrogen flame pyrolysis method, J. Am. Chem. Soc. 128 (2006) 14498–14505.
[19] M. Ahren, L. Selegard, A. Klasson, F. Soderlind, N. Abrikossova, C. Skoglund, T. Bengtsson, M. Engstrom, P. Kall, K. Uvdal, Synthesis and characterization of PEGylated Gd_2O_3 Nanoparticles for MRI Contrast Enhancement, Langmuir 26 (2010) 5753–5762.
[20] W. Rossner, B.C. Grabmaier, Phosphors for X-ray detectors in computed tomography, J. Lumin. 48–49 (1991) 29–36.
[21] B. Vinila, P.D. Dimple, M. Mohapatra, S.V. Godbole, R. Ghildiyal, A.K. Tyagi, Rare-earth doped gadolinia based phosphors for potential multicolor and white light emitting deep UV LEDs, Nanotechnology 20 (2009) 125707.
[22] S.C. Sun, B. Murray, Synthesis of monodisperse cobalt nanocrystals and their assembly into magnetic superlattices, J. Appl. Phys. 85 (1999) 4325–4330.
[23] E. Zych, C. Brecher, A.J. Wojtowicz, H. Lingertat, Luminescence properties of Ce-activated YAG optical ceramic scintillator materials, J. Lumin. 75 (1997) 193–203.
[24] K. Zheng, D. Zhang, D Zhao, N Liu, F. Shi, W. Qin, Bright white upconversion emission from Yb^{3+}, Er^{3+}, and Tm^{3+}-codoped Gd_2O_3 nanotubes, Phys. Chem. Chem. Phys. 12 (2010) 7620–7625.
[25] S. Li, H. Song, H. Yu, S. Lu, X. Bai, G. Pan, Y. Lei, L. Fan, T. Wang, Influence of annealing temperature on photoluminescence characteristics of Gd_2O_3:Eu/AAO nanowires, J. Lumin. 122–123 (2006) 876–878.
[26] S. Seo, H. Yang, P.H. Holloway, Controlled shape growth of Eu or Tb-doped luminescent Gd_2O_3 colloidal nanocrystals, J. Colloid Interface Sci. 331 (2009) 236–242.
[27] Y. Li, G. Hong, Synthesis and luminescence properties of nanocrystalline Gd_2O_3:Eu^{3+} by combustion process, J. Lumin. 124 (2007) 297–301.
[28] M.E. Rabanal, C. Moral, J.M. Torralba, L. Mancic, O. Milosevic, Gd_2O_3:Eu^{3+} phosphor particles processed through aerosol route, J. Eur. Ceram. Soc. 25 (2005) 2023–2027.
[29] Y. Liu, P. Yang, W. Wang, H. Dong, J. Lin, Fabrication and photoluminescence properties of hollow Gd_2O_3:Ln (Ln=Eu^{3+}, Sm^{3+}) spheres via a sacrificial template method, CrystEngComm 12 (2010) 3717–3723.
[30] G. Jia, H. You, K. Liu, Y. Zheng, N. Guo, H. Zhang, Highly uniform Gd_2O_3 hollow microspheres: template directed synthesis and luminescent properties, Langmuir 26 (2010) 5122–5128.
[31] P. Du, L. Song, J. Xiong, Z. Xi, D. Jin, L. Wang, Preparation and the luminescent properties of Tb^{3+}-doped Gd_2O_3 fluorescent nanofibers via electrospinning, Nanotechnology 22 (2011) 035602.
[32] Geo Rajan, K.G. Gopchandran, Enhanced luminescence from spontaneously ordered Gd_2O_3:Eu^{3+} based nanostructures, Appl. Surf. Sci. 255 (2009) 9112–9123.

[33] L.G. Jacobsohn, B.L. Bennett, R.E. Muenchausen, S.C. Tornga, J.D. Thompson, O. Ugurlu, D.W. Cooke, A.L. Lima Sharma, Multifunction Gd_2O_3:Eu nanocrystals produced by solution combustion synthesis: Structural, luminescent, and magnetic characterization, J. Appl. Phys. 103 (2008) 104303.
[34] R.G. Abhilash Kumar, Satoshi Hata, K.G. Gopchandran, Diethylene glycol mediated synthesis of Gd_2O_3:Eu^{3+} nanophosphor and its Judd–Ofelt analysis, Ceram. Int. 39 (2013) 9125–9136.
[35] Y. Sun, Y. Xia, Shape-controlled synthesis of gold and silver nanoparticles, Science 298 (2002) 2176–2179.
[36] D.S. Kilin, O.V. Prezhdo, Y.N. Xia, Shape-controlled synthesis of silver nanoparticles: Ab initio study of preferential surface coordination with citric acid, Chem. Phys. Lett. 458 (2008) 113–116.
[37] A.E. Morales, E.S. Mora, U. Pal, Use of diffuse reflectance spectroscopy for optical characterization of unsupported nanostructures, Rev. Mex. Fis. S53 (5) (2007) 18–22.
[38] K. Nakamoto, Infrared and raman spectra of inorganic and coordination compounds, sixth ed., John Wiley & Sons, New Jersey, 2009.
[39] T. Gougousi, D. Niu, R.W. Ashcraft, G.N. Parsons, Carbonate formation during post-deposition ambient exposure of high-k dielectrics, Appl. Phys. Lett. 83 (2003) 3543–3545.
[40] A. Garcia-Murillo, C.L. Luyer, C. Dujardin, C. Pedrini, J. Mugnier, Elaboration and characterization of Gd_2O_3 waveguiding thin films prepared by the sol–gel process, Opt. Mater. 16 (2001) 39–46.
[41] Y. Repelin, C. Proust, E. Husson, J.M. Beny, Vibrational spectroscopy of the c-form of yttrium sesquioxide, J. Solid State Chem. 118 (1995) 163–169.
[42] W.B. White, V.G. Keramidas, Vibrational spectra of oxides with the c-type rare earth oxide structure, Spectrochem. Acta A 28 (1972) 501–509.
[43] C.L. Luyer, A. Garcia-Murillo, E. Bernstein, J. Mugnier, Waveguide raman spectroscopy of sol–gel Gd_2O_3 thin films, J. Raman Spectrosc. 34 (2003) 234–239.
[44] L. Li, S.Y. Zhang, Dependence of charge transfer energy on crystal structure and composition in Eu^{3+}-doped compounds, J. Phys. Chem. B 110 (2006) 21438–21443.
[45] L. Li, H.K. Yang, B.K. Moon, B.C. Choi, J.H. Jeong, K.H. Kim, Photoluminescent properties of Ln_2O_3:Eu^{3+} (Ln=Y, Lu and Gd) prepared by hydrothermal process and sol–gel method, Mater. Chem. Phys. 119 (2010) 471–477.
[46] C. Wu, W. Qin, G. Qin, D. Zhao, J. Zhang, S. Huang, S. Lu, H. Liu, H. Lin, Photoluminescence from surfactant-assembled Y_2O_3:Eu nanotubes, Appl. Phys. Lett. 82 (2003) 520–522.
[47] G.Z. Li, M. Yu, Z.L. Wang, J. Lin, R.S. Wang, J. Fang, Sol–Gel fabrication and photoluminescence properties of SiO_2@Gd_2O_3:Eu^{3+} core–shell particles, J. Nanosci. Nanotechnol. 6 (2006) 1416–1422.
[48] L. Xu, B. Wei, Z. Zhang, Z. Lu, H. Gao, Y. Zhang, Synthesis and luminescence of europium doped yttria nanophosphors via a sucrose-templated combustion method, Nanotechnology 17 (2006) 4327–4331.
[49] L. Xu, X.Y. Yang, Z. Zhai, X. Chao, Z.H. Zhang, W.H. Hou, EDTA-mediated hydrothermal synthesis of $NaEu(MoO_4)_2$ microrugbies with tunable size and enhanced luminescence properties, CrystEngComm. 13 (2011) 4921–4929.
[50] Z.M. Qi, C.S. Shi, W.W. Zhang, W.P. Zhang, T.D. Hu, Local structure and luminescence of nanocrystalline Y_2O_3:Eu, Appl. Phys. Lett 81 (2002) 2857–2859.
[51] B. Antic, J. Rogan, A. Kremenovic, A.S. Nikolic, M. Vucinic-Vasic, D.K. Bozanic, G.F. Goya, Ph. Colomban, Optimization of photoluminescence of Y_2O_3:Eu and Gd_2O_3:Eu phosphors synthesized by thermolysis of 2,4-pentanedione complexes, Nanotechnology 21 (2010) 245702.
[52] J.C. Boyer, F. Vetrone, J.A. Capobianco, A. Speghini, M.J. Bettinelli, Variation of fluorescence lifetimes and Judd–Ofelt parameters between Eu^{3+} doped bulk and nanocrystalline cubic Lu_2O_3, J. Phys. Chem. B 108 (2004) 20137–20143.
[53] R.W.G. Hunt, Measuring colour: applied science and industrial technology, second ed., Ellis Horwood, New York, 1991.
[54] C.S. McCamy, Correlated color temperature as an explicit function of chromaticity coordinates, Color Research & Application 17 (1992) 142–144.
[55] B.R. Judd, Optical absorption intensities of rare-earth ions, Phy. Rev. 127 (1962) 750–761.
[56] G.S. Ofelt, Intensities of crystal spectra of rare-earth ions, J. Chem. Phy. 37 (1962) 511–520.
[57] M.J. Weber, T.E. Varitimos, B.H. Matsinger, Optical intensities of rare-earth ions in yttrium orthoaluminate, Phys. Rev. B 8 (1973) 47–53.
[58] J. Guan, B. Chen, Y. Sun, H. Liang, Q. Zhang, Effects of synergetic ligands on the thermal and radiative properties of $Eu(TTA)_3$nL-doped poly(methyl methacrylate), J. Non-Cryst. Solids 351 (2005) 849–855.